IN-34
146075
P-14

NASA Technical Memorandum 4411

Computational Parametric Study of Sidewall-Compression Scramjet Inlet Performance at Mach 10

Scott D. Holland

FEBRUARY 1993

(NASA-TM-4411) COMPUTATIONAL PARAMETRIC STUDY OF SIDEWALL-COMPRESSION SCRAMJET INLET PERFORMANCE AT MACH 10 (NASA) 14 p

N93-20299

Unclas

H1/34 0146075

NASA

NASA Technical Memorandum 4411

Computational Parametric Study of Sidewall-Compression Scramjet Inlet Performance at Mach 10

Scott D. Holland
Langley Research Center
Hampton, Virginia

National Aeronautics and
Space Administration
Office of Management
Scientific and Technical
Information Program
1993

Abstract

A computational parametric study of three-dimensional, sidewall-compression scramjet inlets was performed to identify the effects of geometric parameters on inlet performance. The parameters were the leading-edge sweep angle, varied between 30° and 60°, and the leading-edge position of the cowl, located at the throat and at two forward positions. A laminar boundary layer with cold-wall (T_{wall} = 300 K (540°R)) boundary conditions was imposed. The parametric study was performed for a Mach number of 10 and a unit free-stream Reynolds number of 7.06 × 10^6 per meter (2.15 × 10^6 per foot) at a geometric contraction ratio of 5. The performance of each configuration was evaluated in terms of the mass capture, throat Mach number, total pressure recovery, kinetic energy efficiency, and internal compression. One computation of an unswept configuration was included as a baseline to determine the effects of introducing leading-edge sweep on the flow-field parameters. The purpose of the computational parametric study was to perform a trade-off of the effects of various geometric parameters on the global performance of the inlet. Although no single optimal configuration emerged, trade-offs among the stated performance parameters identified a leading-edge sweep angle of 45° as possessing the most attractive performance characteristics.

Symbols

A	inlet throat area, cm^2 (in^2)
CR	contraction ratio, W/g
$C_{x'}$	distance from throat entrance to cowl leading edge, cm (in.)
g	throat gap, cm (in.)
H	height of inlet, 18.3 cm (7.2 in.)
L	length of model, 78.7 cm (31 in.)
M	Mach number
M_∞	free-stream Mach number
$\overline{M}$	momentum-averaged throat Mach number, $\frac{\iint \rho u^2 M \, dA}{\iint \rho u^2 \, dA}$
m_c	percent mass capture, $\frac{\dot{m}_{\text{throat}}}{\dot{m}_{\text{ent}}}$
$\dot{m}_{\text{ent}}$	mass flow rate at inlet entrance, kg/s (lbm/s)
$\dot{m}_{\text{throat}}$	mass flow rate at inlet throat, kg/s (lbm/s)
p	static pressure, Pa (psia)
p_∞	free-stream static pressure, Pa (psia)
$\overline{p}$	area-weighted compression, $\frac{\iint p \, dA}{p_\infty \iint dA}$
$\overline{p}_r$	momentum-averaged total pressure recovery, $\frac{\iint \rho u^2 p_t \, dA}{p_{t,\infty} \iint \rho u^2 \, dA}$
p_t	total pressure, Pa (psia)
$p_{t,\infty}$	free-stream total pressure, Pa (psia)
R_∞	free-stream Reynolds number
T	temperature, K (°R)
T_{wall}	wall temperature, 300 K (540°R)
$T_{x'}$	distance from sidewall leading edge to constant-area throat entrance, cm (in.)
T_∞	free-stream temperature, K (°R)
u	axial velocity, m/s (ft/s)
W	inlet width at sidewall leading edge, cm (in.)
x'	axial distance measured from sidewall leading edge, cm (in.)
γ	ratio of specific heats
δ	sidewall-compression angle, deg
η_c	adiabatic compression efficiency, $1 - \frac{\gamma - 1}{2} M_\infty^2 \left(\frac{1 - \eta_{KE}}{\chi - 1} \right)$

η_{KE} kinetic energy efficiency, $1 - \left[\frac{\left(\frac{p_{t,\infty}}{p_t}\right)^{\frac{\gamma-1}{\gamma}} - 1}{\left(\frac{\gamma-1}{2}\right) M_\infty^2} \right]$

Λ leading-edge sweep angle, deg

ρ density, kg/m^3 (lbm/ft^3)

χ momentum-averaged static temperature ratio, $\frac{\iint \rho u^2 T \, dA}{T_\infty \iint \rho u^2 \, dA}$

Introduction

The advantages and design requirements of propulsion-airframe integration for high Mach number flight have led to extensive study of the three-dimensional, sidewall-compression scramjet inlet. Recent research publications have reported tests over a broad range of Mach numbers (2 to 18) in a variety of test gases. Inlets of this genre have been studied experimentally in the past for the overall performance characteristics (at Mach numbers between 2 and 6) and as part of a subscale engine system by Trexler (refs. 1 through 3) and Trexler and Souders (ref. 4). The inlets have been studied more recently in a variety of test gases and over a broad range of Mach numbers—Mach 4 (in air) by Kanda et al. (ref. 5); Mach 18 and 22 (in helium) by Trexler (ref. 2); and Mach 6 (in tetrafluoromethane) by Holland and Perkins (ref. 6). The works of Kanda et al. (ref. 5) at Mach 4 (in air) and Vinogradov et al. (ref. 7) at Mach 2 through 6 (in air) also demonstrate an interest in sidewall-compression inlets by the Japanese and Soviets, respectively.

Recent work has also highlighted the use of computational fluid dynamics (CFD) for inlet research. Kumar (ref. 8) has developed and evolved a three-dimensional Navier-Stokes code primarily for internal flow configurations. Favorable comparisons between experimental data and computational results from this code have been presented by Kumar and Trexler (ref. 9) for a generic scramjet engine configuration at a nominal Mach number of 4. Computational analyses of subscale engines and combustion processes have also been performed. Srinivasan, McClinton, and Kamath (ref. 10) have presented results from a version of the code which computed the three-dimensional, turbulent, reacting flow through the entire Langley parametric scramjet engine at an inflow Mach number of 6.25. Sekar, Thomas, and Srinivasan (ref. 11) have used the code to compute flow in one of the Mach 6 nozzles from the Langley Arc-Heated Scramjet Test Facility and subsequently through the parametric scramjet inlet. Kumar, Singh, and Trexler (ref. 12) have performed a numerical study of the effects of reverse sweep on scramjet inlet performance at Mach 4.5. One advantage of CFD is the provision of flow-field data, whereas experimental data are typically limited to surface measurements or global flow-field techniques such as vapor screens or schlieren photography. White, Drummond, and Kumar (ref. 13) point out that CFD yields parametric studies in a timely and cost-effective manner, and when wind-tunnel data are obtained, aids in the explanation of unusual or unexpected phenomena by providing detailed flow-field data. Additionally, the ability of the code to match the experimental surface measurements gives the designer greater confidence in the computed flow-field data.

Because CFD has demonstrated reliability in certain applications as an engineering design tool, the present work applies CFD in this preliminary design capacity. In support of projects such as the National Aero-Space Plane (X-30), a combined computational and experimental parametric study of the internal aerodynamics of a generic three-dimensional sidewall-compression scramjet inlet has been undertaken. Because instrumented wind-tunnel models are quite expensive, CFD is applied in this study to minimize the fabrication costs by eliminating designs that promise poor performance. The purpose of this work is to perform a trade-off study of the effects of various geometric parameters on the global performance of the inlet. A wind-tunnel model, based on the design derived from the present work, will be fabricated and tested to provide a detailed comparison with computational prediction. Therefore, the boundary conditions were chosen to match the anticipated test environment of the Langley 31-Inch Mach 10 Tunnel: a laminar boundary layer with constant 300 K (540°R) wall temperature.

Configuration Description and Parametric Variations

The present configuration was adopted for this Mach 10 parametric study from a sparse computational and experimental data base available for lower supersonic Mach numbers. The inlet sidewalls were a constant 18.3 cm (7.2 in.) in height H and 78.7 cm (31 in.) in total length L (see fig. 1). The baseplate extended only 2.5 cm (1 in.) ahead of the sidewall leading edge. Therefore, no entrance boundary layer was present, and the configuration modeled an uninstalled inlet. The distance from the sidewall leading edge to the constant-area throat $T_{x'}$ was 57.9 cm (22.8 in.). Leading-edge sweep angles Λ

between 30° and 60° were selected for this parametric study to represent a range of moderately to highly swept cases. A configuration with a sidewall leading-edge sweep angle of 0° was also included to determine the effects of introducing sweep angle on performance. The sidewall-compression angle δ was fixed at 6°. This value was selected from a trade study (ref. 4) as a compromise between larger compression angles, which lead to stronger shocks and an increased probability of boundary-layer separation and smaller compression angles, which require a longer inlet, thus imposing a size and weight penalty to obtain the same compression. In general, the contraction ratio CR is the ratio of the inlet entrance area to the throat area. The inlet height, length, and sidewall compression result in a contraction ratio of 5 for the present case. The cowl position $C_{x'}$ was the distance between the cowl leading edge and the start of the throat region (fig. 1); the length $T_{x'}$ was the distance between the constant-area throat and the sidewall leading edge. The ratio $C_{x'}/T_{x'}$ defines the forward extent of the cowl ahead of the throat as a percentage of the length of the compression surface. Therefore, $C_{x'}/T_{x'} = 0.50$ (referred to as a 50-percent cowl) indicated that the cowl leading edge was moved forward halfway between the beginning of the throat and the sidewall leading edge. Likewise, $C_{x'}/T_{x'} = 0.25$ (a 25-percent cowl) indicated that the cowl leading edge was forward of the throat by one-quarter of the distance between the throat and sidewall leading edge. Finally, $C_{x'}/T_{x'} = 0.00$ (a 0-percent cowl) indicated that the cowl leading edge was at the throat.

Inlet Code

The three-dimensional Navier-Stokes code SCRAMIN described in reference 8 was adapted for the present parametric study. The code solves the governing equations in full-conservation form using MacCormack's time-asymptotic, explicit, predictor-corrector method (ref. 14). This method is second-order accurate in time and space and yields to a high degree of vectorization. The present work employed an algebraic grid generation technique with linear connecting functions, described in reference 15, to obtain the Jacobian and metric data. The grid refinement function of reference 16 was included in the transformation for the y and z coordinates to cluster the grid points near the boundaries in the physical domain. The computational mesh possesses 80 grid points in the axial direction, 31 points in the lateral direction, and 61 points in the vertical direction (46 points inside the inlet and 15 points beneath the cowl plane for the flow spillage). A check on grid independence was performed by a 50-percent increase in the grid density in all three coordinate directions for the extreme cases of $\Lambda = 30°$ with 0-percent cowl and $\Lambda = 60°$ with 50-percent cowl. Besides a substantial increase in CPU time, the grid refinement had no significant effect on the integrated performance quantities; for example, $\overline{p}_r$ varied by less than 0.1 percent.

Shock/boundary-layer interactions depend on the size and character of the incoming boundary layer. The present configuration, however, modeled an uninstalled inlet, i.e., no incoming boundary layer was imposed at the inflow boundary. The inflow boundary was maintained at free-stream conditions while an extrapolation boundary condition was applied at the exit plane. On solid surfaces, all velocity components and the normal pressure gradient were required to be identically zero. A constant temperature distribution ($T_{\text{wall}} = 300$ K (540°R)) provided the thermal boundary condition. Open boundaries were calculated assuming vanishing normal gradients in velocity, temperature, and pressure. Because the flow field was symmetric, only half the field was computed, and symmetry boundary conditions were imposed. The initial conditions were given by assigning free-stream conditions to each grid point except those at the boundaries, where appropriate boundary conditions were applied.

Results

A discussion of the general trends is presented for each flow-field parameter: mass capture, throat Mach number, total pressure recovery, kinetic energy efficiency, and internal compression. Because these parameters may vary considerably across the exit plane, the determination of a single representative (average) number can obscure the true complexity of the flow field. Nevertheless, average values are presented to compare performance. These results are presented for the free-stream conditions given in table I. In addition to the range of leading-edge sweep angle, a single configuration with a 0-percent cowl and a sidewall leading-edge sweep angle of 0° was computed to identify explicitly the effects of introducing sweep. Table II is a tabular summary of the performance parameters. The table also includes the static temperature ratio as well as the adiabatic compression efficiency for reference.

Mass Capture

Figure 2 presents the effects of leading-edge sweep angle and cowl position on mass capture m_c. In general, the mass capture decreases with an increase in leading-edge sweep angle. As noted in reference 17,

aft leading-edge sweep promotes the turning of the flow toward the cowl plane. This increase in spillage appears as a decrease in mass capture. Reference 17 also notes that the effect of forward cowl position is the capture of the flow that otherwise would have spilled ahead of the cowl. Significant effort was expended to identify the shape of the curve for the 0-percent cowl configuration. The mass capture was observed to decrease monotonically in an almost parabolic fashion. Changing the leading-edge sweep angle from 0° to 30° has an almost negligible effect on mass capture, yet sweeping the leading edge beyond an angle of 30° has an increasing and significant effect on the rate at which mass capture decreases with the leading-edge sweep angle.

Throat Mach Number

Figure 3 presents the variation of the momentum-averaged throat Mach number $\overline{M}$ with leading-edge sweep angle and cowl position. The throat Mach number increases with leading-edge sweep and decreases with forward cowl position. As the leading-edge sweep angle increases, the strength of the leading-edge shock appears to decrease, which yields a higher postshock Mach number. This effect is not expected from inviscid considerations. In fact, Holland and Perkins (ref. 18) demonstrated that the inviscid shock strength for a swept inlet configuration is invariant with leading-edge sweep because of the compensating effects of decreased normal Mach number and increased effective wedge angle (the sidewall-compression angle measured normal to the leading edge) with increased sweep angle. An increase in leading-edge sweep angle appears to decrease the displacement effects of the sidewall boundary layer by means of flow turning and spillage; thus, the net effect is a decreased shock strength. A forward cowl position, however, lowers the throat Mach number because of the shock formed on the cowl. The cowl shock extends farther into the exit plane for a forward placement of the cowl leading edge than it does for an aft placement. Because more of the exit plane is affected by the cowl shock, the average throat Mach number decreases. Comparison of the throat Mach number for a configuration with a sweep angle of 30° with that for a sweep angle of 0° indicates that below 30° no sudden change occurs in the rate at which the throat Mach number decreases. For example, the rate of change in Mach number is nearly the same for a leading-edge sweep angle between 30° and 35° as for one between 0° and 30°. This outcome indicates that the change in average Mach number per degree of leading-edge sweep asymptotically approaches a constant value.

Total Pressure Recovery and Kinetic Energy Efficiency

Figure 4 indicates that the momentum-averaged total pressure recovery $\overline{p}_r$ increases with leading-edge sweep angle. As noted previously, the shock sheets generated from the swept sidewall leading edges become weaker as the sweep increases. This weakening yields a higher total pressure recovery in the postshock region. The forward placement of the cowl lowers the average total pressure recovery due to the cowl shock formed on the leading edge, just as the average throat Mach number decreases as the cowl is moved forward. These conditions occur for a leading-edge sweep angle of 30°; however, as the leading-edge sweep angle increases, the effect of the cowl placement reverses. The average total pressure recovery for a leading-edge sweep angle of 60° increases with forward cowl placement. This increase indicates a complex interaction that is partially obscured by the averaging process. With the increase in leading-edge sweep angle comes a significant increase in spillage. The flow that spills is the high-pressure, high-velocity flow near the cowl, whereas the low-momentum boundary-layer flow is captured for each sweep angle. Because the mass capture is smaller for increased sweep angles, the boundary-layer flow occupies an increasingly larger proportion of the flow captured by the inlet. The increased proportion of the boundary-layer flow, when averaged over the exit plane, yields an effective decrease in total pressure recovery of the inlet. When the cowl is brought forward, more of the high-momentum compressed core flow is captured. On average, despite the strengthened cowl shock, the increased capture yields a net increase in total pressure recovery. At large leading-edge sweep angles, the effect of sweep on total pressure recovery is significant; as the leading-edge sweep angle decreases toward zero, the per-degree change in total pressure recovery appears to approach a constant at a sweep angle of 35°, i.e., the rate of decrease between a sweep angle between 35° and 30° is the same as that between 30° and 0°.

Figure 5 shows the effect of leading-edge sweep angle and cowl position on kinetic energy efficiency η_{KE}. For each configuration, the kinetic energy efficiency exceeded 98 percent and increased with an increase of the leading-edge sweep angle for each of the cowl positions. Because of the functional relationship between total pressure recovery and kinetic energy efficiency, the kinetic energy efficiency follows the same trends as the total pressure recovery. The parameter η_{KE} is commonly used to compare performance among candidate inlet configurations and is provided in table II for reference. Likewise,

the momentum-averaged static temperature ratio χ and the adiabatic compression efficiency η_c are also included for reference.

Area-Weighted Compression

Figure 6 indicates that for all the configurations considered, the inlet area-weighted compression $\overline{p}$ varied from 15 to 22. The compression is observed to decrease with an increase in leading-edge sweep angle caused by both the weakened swept internal shocks and the spillage of increased high-pressure flow near the cowl plane. At the forward cowl positions, the loss of some high-pressure fluid is compensated by the compression from the cowl shock. Although the cowl shock strength is insufficient to cause an increase in the average compression, the rate of degradation of average compression with respect to the leading-edge sweep angle decreases. Because spillage is minimized when the leading-edge sweep angle tends toward zero, loss of the high-pressure fluid is minimized; thus, a reduction in leading-edge sweep angle from 30° to 0° yields less change in compression than the reduction from 60° to 30°.

Concluding Remarks

Some of the most important inlet parameters are mass capture, total pressure recovery, kinetic energy efficiency, and internal compression. This study showed that, compared with an unswept configuration, the inlet sidewalls could be swept by an angle of up to 30° without adversely affecting the inlet performance. Because the addition of leading-edge sweep angle caused an increase in flow spillage, the swept configurations are expected to possess better low Mach number starting performance. The mass capture decreased with an increase in sidewall leading-edge sweep angle because the sweep promoted flow turning toward the cowl. Forward placement of the cowl leading edge increased the mass capture by preventing the flow from spilling. The forward cowl position increased the average compression of the inlet exit plane via the cowl shock, at a cost of additional flow nonuniformity and decreased total pressure recovery. The desired optimal configuration would simultaneously possess relative maxima in compression, mass capture, total pressure recovery, and kinetic energy efficiency at a given leading-edge sweep angle. Because the behavior of these parameters with leading-edge sweep angle increases or decreases monotonically, a mathematical optimum cannot be obtained; thus, any selection of an optimized configuration must be made by trade-offs. The configuration with a sweep angle of 60° exhibited a significantly lower mass capture and internal compression than that of the 45° configuration but provided a much higher total pressure recovery and kinetic energy efficiency. To maintain the same geometric contraction, an increase in leading-edge sweep angle requires an increase in length (hence weight), which is undesirable for an engine component. The 45° configuration displayed nearly the same mass capture and internal compression as the 30° configuration and demonstrated a 5- to 7-percent improvement in total pressure recovery. Although no single optimal configuration clearly emerged from this study, the configuration with a leading-edge sweep angle of 45° appears to exhibit the most promising performance characteristics after considering the trade-offs among mass capture, total pressure recovery, kinetic energy efficiency, and internal compression.

NASA Langley Research Center
Hampton, VA 23681-0001
November 25, 1992

References

1. Trexler, Carl A.: Inlet Performance of the Integrated Langley Scramjet Module (Mach 2.3 to 7.6). AIAA Paper No. 75-1212, Sept.–Oct. 1975.

2. Trexler, Carl A.: *Tests of Two Sidewall-Compression Scramjet Inlets at Mach 18.1 to 21.6 in Helium.* NASP TM-1018, 1988.

3. Trexler, Carl A.: Inlet Starting Predictions for Sidewall-Compression Scramjet Inlets. AIAA-88-3257, July 1988.

4. Trexler, Carl A.; and Souders, Sue W.: *Design and Performance at a Local Mach Number of 6 of an Inlet for an Integrated Scramjet Concept.* NASA TN D-7944, 1975.

5. Kanda, T.; Komuro, T.; Masuya, G.; Kudo, K.; Murakami, A.; Tani, K.; Wakamatsu, Y.; and Chinzei, N.: Mach 4 Testing of Scramjet Inlet Model. AIAA-89-2680, July 1989.

6. Holland, Scott D.; and Perkins, John N.: Mach 6 Testing of Two Generic Three-Dimensional Sidewall Compression Scramjet Inlets in Tetrafluoromethane. AIAA-90-0530, Jan. 1990.

7. Vinogradov, V. A.; Stepanov, V. A.; and Alexandrovich, E. V.: Numerical and Experimental Investigation of Airframe-Integrated Inlet for High Velocities. AIAA-89-2679, July 1989.

8. Kumar, Ajay: *Numerical Simulation of Scramjet Inlet Flow Fields.* NASA TP-2517, 1986.

9. Kumar, Ajay; and Trexler, Carl A.: Analysis and Performance Prediction of Scramjet Inlets Utilizing a Three-Dimensional Navier-Stokes Code. *Langley Symposium on Aerodynamics,* Volume I, Sharon H. Stack, compiler, NASA CP-2397, 1985, pp. 187–208.

10. Srinivasan, S.; McClinton, C. R.; and Kamath, P. S.: Numerical Simulation of Flow Through the Langley Parametric Scramjet Engine. SAE Tech. Paper Ser. 892314, Sept. 1989.

11. Sekar, B.; Thomas, S.; and Srinivasan, S.: A Numerical Parametric Study of a Scramjet Inlet in a Mach 6 Arc Heated Test Facility. AIAA-90-0531, Jan. 1990.

12. Kumar, Ajay; Singh, D. J.; and Trexler, Carl A.: Numerical Study of the Effects of Reverse Sweep on Scramjet Inlet Performance. *J. Propuls. & Power,* vol. 8, no. 3, May–June 1992, pp. 714–719.

13. White, M. E.; Drummond, J. P.; and Kumar, A.: Evolution and Application of CFD Techniques for Scramjet Engine Analysis. *J. Propuls. & Power,* vol. 3, no. 5, Sept.–Oct. 1987, pp. 423–439.

14. MacCormack, Robert W.: The Effect of Viscosity in Hypervelocity Impact Cratering. AIAA Paper No. 69-354, Apr.–May 1969.

15. Smith, R. E.: *Two-Boundary Grid Generation for the Solution of the Three-Dimensional Compressible Navier-Stokes Equations.* NASA TM-83123, 1981.

16. Roberts, Glyn O.: Computational Meshes for Boundary Layer Problems. *Proceedings of the Second International Conference on Numerical Methods in Fluid Dynamics, Volume 8 of Lecture Notes in Physics,* Maurice Holt, ed., Springer-Verlag, 1971, pp. 171–177.

17. Holland, Scott D.: A Computational and Experimental Investigation of a Three-Dimensional Hypersonic Scramjet Inlet Flow Field. Ph.D. Diss., North Carolina State Univ., 1991.

18. Holland, Scott D.; and Perkins, John N.: Internal Shock Interactions in Propulsion/Airframe Integrated Three-Dimensional Sidewall Compression Scramjet Inlets. AIAA-92-3099, July 1992.

Table I. Flow Conditions for Langley 31-Inch Mach 10 Tunnel

Stagnation:

$p_{t,1}$, N/m^2 (psi)	9.997×10^6 (1450)
$T_{t,1}$, K (°R)	1005 (1810)

Free stream:

M_∞	10.05
p_∞, N/m^2 (psi)	224.2 (0.0325)
T_∞, K (°R)	49.7 (89.4)
ρ_∞, kg/m^3 (slug/ft^3)	0.0157 (3.053×10^{-5})
u_∞, m/s (ft/s)	1420 (4660)
R_∞, per meter (per foot)	7.06×10^6 (2.15×10^6)

Table II. Performance Parameters for Computational Parametric Study

Leading-edge sweep, Λ, deg	Percent mass capture, m_c	Throat Mach number, $\overline{M}$	Total pressure recovery, $\overline{p}_r$	Kinetic energy efficiency, η_{KE}	Area-weighted compression, $\overline{p}$	Static temperature ratio, χ	Adiabatic compression efficiency, η_c
0-percent cowl							
0	96.73	5.202	0.443	0.9869	19.91	3.386	0.8902
30	96.05	5.345	.443	.9869	18.78	3.249	.8835
35	95.70	5.369	.445	.9870	18.65	3.236	.8836
40	94.99	5.410	.452	.9873	18.31	3.198	.8841
45	94.05	5.449	.461	.9876	18.00	3.173	.8860
50	92.92	5.483	.472	.9880	17.50	3.144	.8884
55	91.42	5.545	.483	.9884	16.74	3.086	.8892
60	88.51	5.623	.499	.9890	15.66	3.034	.8920
25-percent cowl							
30	98.28	5.227	0.439	0.9867	20.45	3.397	0.8894
45	96.90	5.303	.455	.9874	19.95	3.354	.8928
60	94.03	5.516	.514	.9895	18.75	3.201	.9048
50-percent cowl							
30	99.41	5.176	0.431	0.9864	21.12	3.449	0.8890
45	98.26	5.256	.452	.9873	20.74	3.411	.8944
60	96.65	5.507	.522	.9898	18.91	3.220	.9081

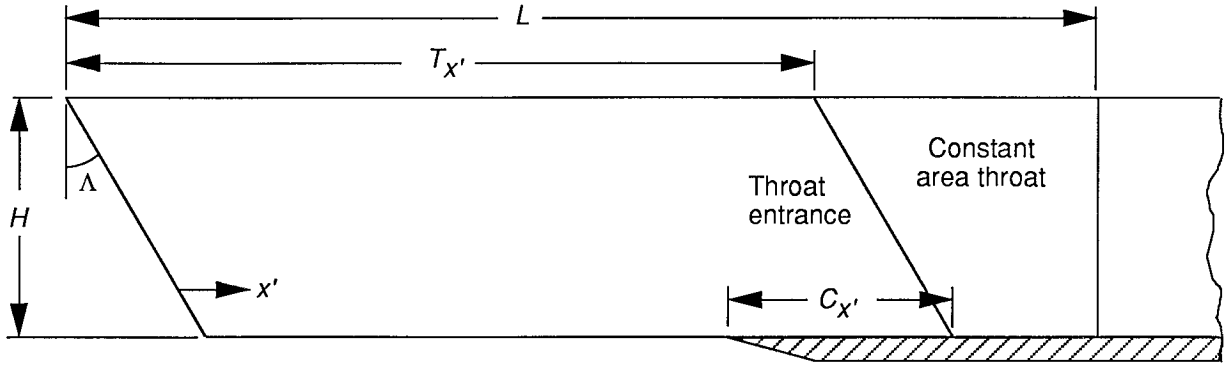

(a) Section A-A: Side view (with cowl).

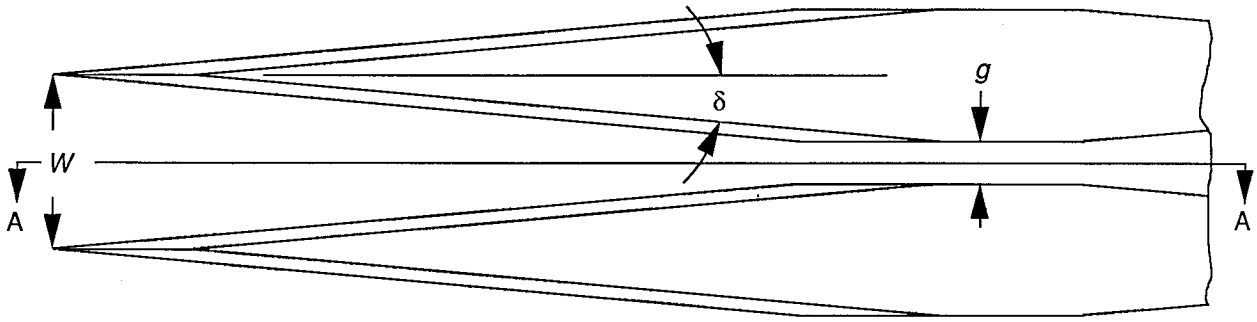

(b) Bottom view (cowl removed).

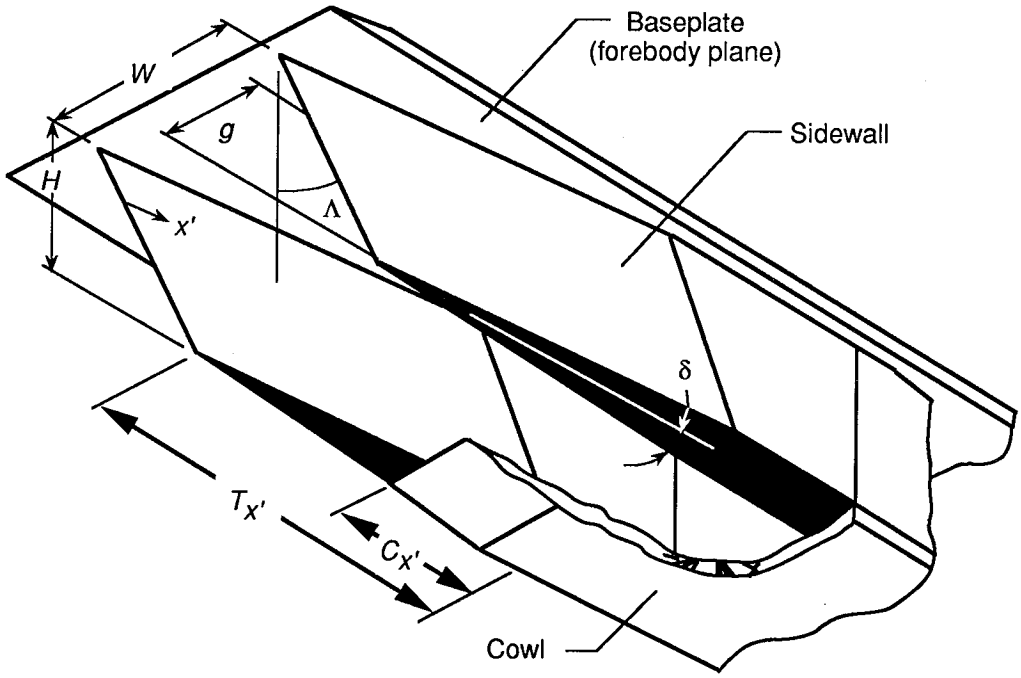

(c) Orthogonal view of inlet configuration in flight orientation.

Figure 1. Inlet configuration.

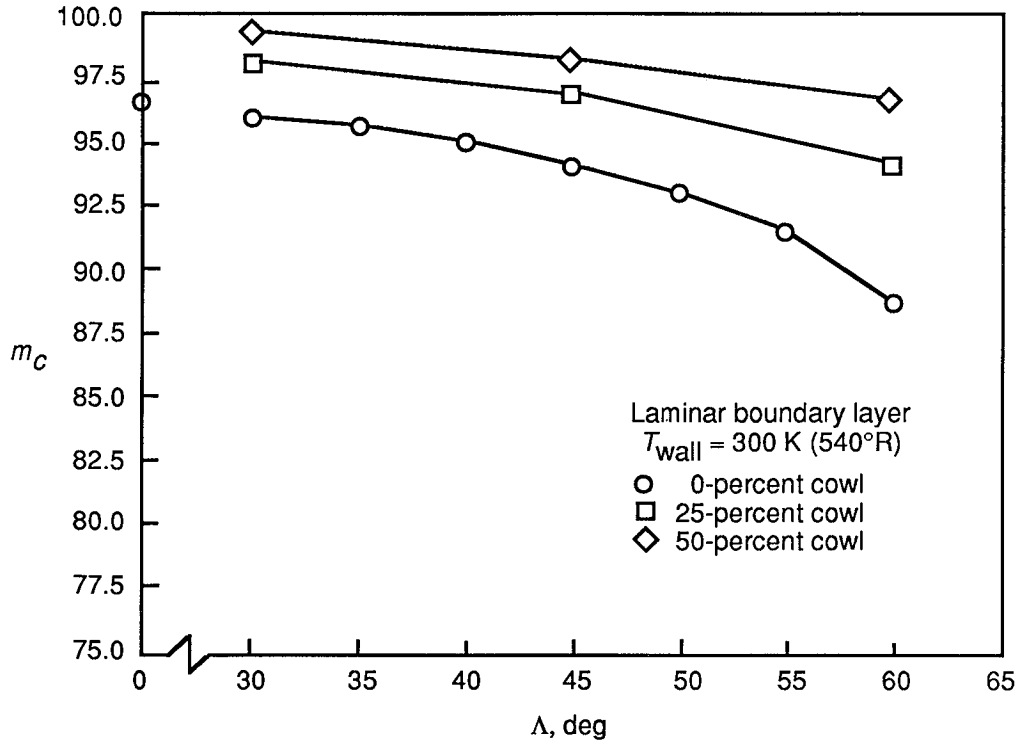

Figure 2. Leading-edge sweep angle and cowl position effects on inlet mass capture.

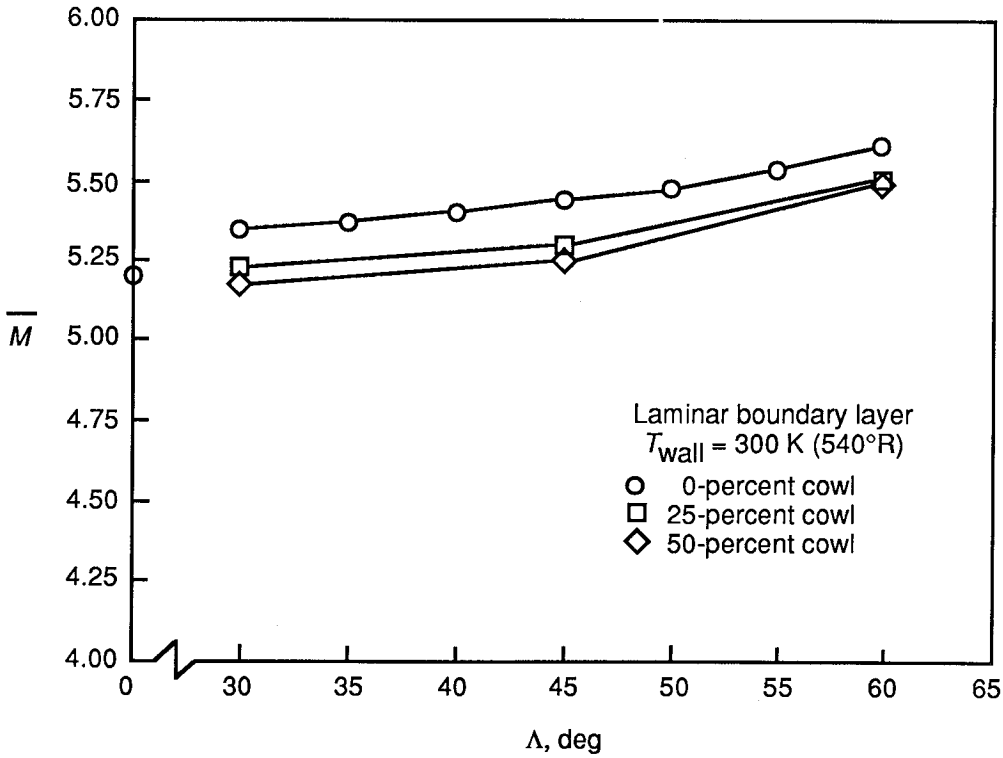

Figure 3. Leading-edge sweep angle and cowl position effects on momentum-averaged throat Mach number.

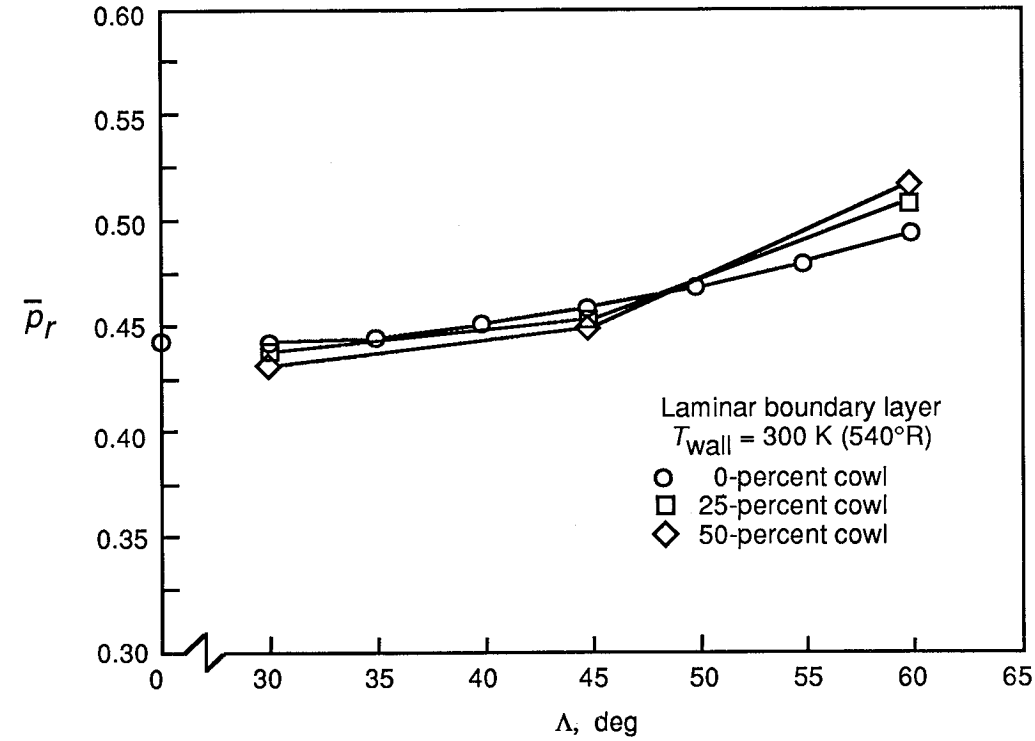

Figure 4. Leading-edge sweep angle and cowl position effects on momentum-averaged total pressure recovery.

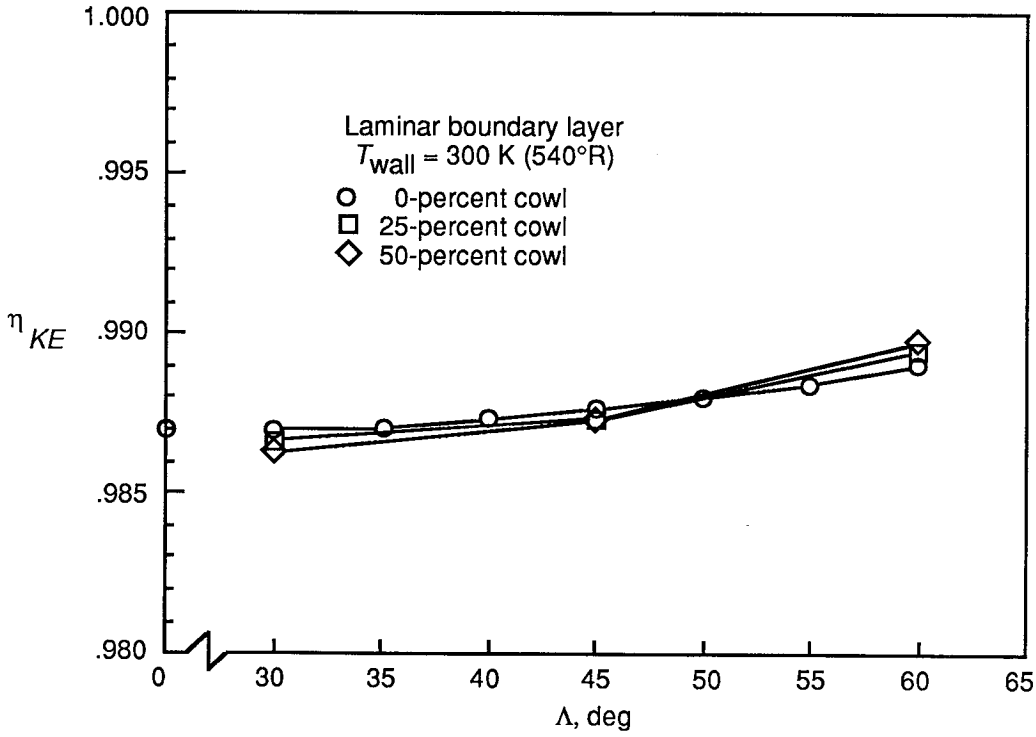

Figure 5. Leading-edge sweep angle and cowl position effects on kinetic energy efficiency.

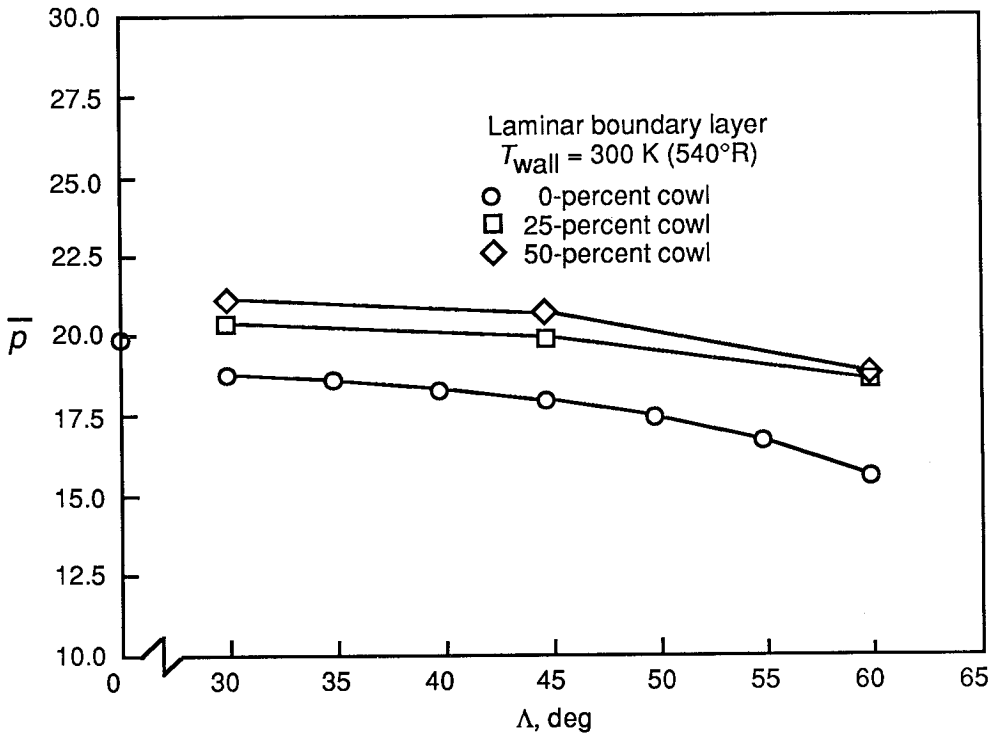

Figure 6. Leading-edge sweep angle and cowl position effects on inlet area-weighted compression.

REPORT DOCUMENTATION PAGE

Form Approved
OMB No. 0704-0188

Public reporting burden for this collection of information is estimated to average 1 hour per response, including the time for reviewing instructions, searching existing data sources, gathering and maintaining the data needed, and completing and reviewing the collection of information. Send comments regarding this burden estimate or any other aspect of this collection of information, including suggestions for reducing this burden, to Washington Headquarters Services, Directorate for Information Operations and Reports, 1215 Jefferson Davis Highway, Suite 1204, Arlington, VA 22202-4302, and to the Office of Management and Budget, Paperwork Reduction Project (0704-0188), Washington, DC 20503.

1. AGENCY USE ONLY *(Leave blank)*	2. REPORT DATE	3. REPORT TYPE AND DATES COVERED
	February 1993	Technical Memorandum

4. TITLE AND SUBTITLE
Computational Parametric Study of Sidewall-Compression Scramjet Inlet Performance at Mach 10

5. FUNDING NUMBERS
WU 506-40-71-04

6. AUTHOR(S)
Scott D. Holland

7. PERFORMING ORGANIZATION NAME(S) AND ADDRESS(ES)
NASA Langley Research Center
Hampton, VA 23681-0001

8. PERFORMING ORGANIZATION REPORT NUMBER
L-17134

9. SPONSORING/MONITORING AGENCY NAME(S) AND ADDRESS(ES)
National Aeronautics and Space Administration
Washington, DC 20546-0001

10. SPONSORING/MONITORING AGENCY REPORT NUMBER
NASA TM-4411

11. SUPPLEMENTARY NOTES

12a. DISTRIBUTION/AVAILABILITY STATEMENT
Unclassified–Unlimited

Subject Category 34

12b. DISTRIBUTION CODE

13. ABSTRACT *(Maximum 200 words)*

A computational parametric study of three-dimensional, sidewall-compression scramjet inlets was performed to identify the effects of geometric parameters on inlet performance. The parameters were the leading-edge sweep angle, varied between 30° and 60°, and the leading-edge position of the cowl, located at the throat and at two forward positions. A laminar boundary layer with cold-wall (T_{wall} = 300 K (540°R)) boundary conditions was imposed. The parametric study was performed for a Mach number of 10 and a unit free-stream Reynolds number of 7.06×10^6 per meter (2.15×10^6 per foot) at a geometric contraction ratio of 5. The performance of each configuration was evaluated in terms of the mass capture, throat Mach number, total pressure recovery, kinetic energy efficiency, and internal compression. One computation of an unswept configuration was included as a baseline to determine the effects of introducing leading-edge sweep on the flow-field parameters. The purpose of the computational parametric study was to perform a trade-off of the effects of various parameters on the global performance of the inlet. Although no single optimal configuration emerged, trade-offs among the stated performance parameters identified a leading-edge sweep angle of 45° as possessing the most attractive performance characteristics.

14. SUBJECT TERMS
Hypersonics; Inlets; Computational fluid dynamics (CFD); Shock interactions

15. NUMBER OF PAGES
12

16. PRICE CODE
A03

17. SECURITY CLASSIFICATION OF REPORT	18. SECURITY CLASSIFICATION OF THIS PAGE	19. SECURITY CLASSIFICATION OF ABSTRACT	20. LIMITATION OF ABSTRACT
Unclassified	Unclassified		

NSN 7540-01-280-5500

Standard Form 298(Rev. 2-89)
Prescribed by ANSI Std. Z39-18
298-102

NASA-Langley, 1993